Original Research *Featured Article*

Immunomodulatory effect of hemozoin on pneumocyte apoptosis via *CARD9* pathway, a possibly retarding pulmonary resolution

Sitang Maknitikul[1], Natthanej Luplertlop[2], Urai Chaisri[1], Yaowapa Maneerat[1] and Sumate Ampawong[1]

[1]Department of Tropical Pathology, Faculty of Tropical Medicine, Mahidol University, Ratchathewi, Bangkok 10400, Thailand;
[2]Department of Microbiology and Immunology, Faculty of Tropical Medicine, Mahidol University, Ratchathewi, Bangkok 10400, Thailand
Corresponding author: Sumate Ampawong. Email: am_sumate@hotmail.com

Impact statement

The present work shows the physical and immunomodulatory properties of hemozoin on the induction of pneumocyte apoptosis in relation to IL-1β production through the *CARD9* pathway. This occurrence may be a possible pathway for the retardation of lung resolution leading to blood–gas-barrier breakdown. Our findings lead to the understanding of the host–parasite relationship focusing on the dysfunction in ALI induced by HZ, a possible pathway of the recovering lung epithelial retardation in malaria-associated ARDS.

Abstract

Plasmodium falciparum, the most virulent malaria parasite species, causes severe symptoms especially acute lung injury (ALI), of which characterized by alveolar epithelium and endothelium destruction and accelerated to blood–gas-barrier breakdown. Parasitized erythrocytes, endothelial cells, monocytes, and cytokines are all involved in this mechanism, but hemozoin (HZ), the parasitic waste from heme detoxification, also mainly contributes. In addition, it is not clear why type II pneumocyte proliferation, alveolar restorative stage, is rare in malaria-associated ALI. To address this, *in vitro* culture of A549 cells with *Plasmodium* HZ or with interleukin (IL)-1β triggered by HZ and monocytes (HZ-IL-1β) was conducted to determine their alveolar apoptotic effect using ethidium bromide/acridine orange staining, annexin-V-FITC/propidium iodide staining, and electron mircroscopic study. Caspase recruitment domain-containing protein 9 (*CARD9*), the apoptotic regulator gene, and IL-1β were quantified by reverse-transcriptase PCR. Junctional cellular defects were characterized by immunohistochemical staining of E-cadherin. The results revealed that cellular apoptosis and *CARD9* expression levels were extremely high 24 h after induction by HZ-IL-1β when compared to the HZ- and non-treated groups. E-cadherin was markedly down-regulated by HZ-IL-1β and HZ treatments. *CARD9* expression was positively correlated with IL-1β expression and the number of apoptotic cells. Interestingly, the localization of HZ in the vesicular surfactant of apoptotic pneumocyte was also identified and submitted to be a cause of alveolar resolution abnormality. Thus, HZ triggers monocytes to produce IL-1β and induces pneumocyte type II apoptosis through *CARD9* pathway in association with down-regulated E-cadherin, which probably impairs alveolar resolution in malaria-associated ALI.

Keywords: Acute lung injury, apoptosis, *CARD9*, hemozoin, interleukin-1β

***Experimental Biology and Medicine* 2018; 243: 395–407. DOI: 10.1177/1535370218757458**

Introduction

Undeniably, there are several complications in severe malaria such as cerebral malaria, acidosis, jaundice, pulmonary edema, hypoglycemia, hyperparasitemia, shock, renal failure, and severe anemia.[1] Severe malaria pathogenesis is generally caused by the parasitized erythrocyte, which induces inflammatory responses, intravascular obstruction with concomitant cellular destruction. Consequential events, particularly tissue hypoxia, ischemia, and necrosis result from parasitized erythrocyte sequestration.[2,3] In the lungs, these conditions are closely related to malaria-associated acute respiratory distress syndrome (ARDS).[4,5] In addition, ARDS, the most severe form of acute lung injury (ALI),[6] is represented by acute onset, non-cardiogenic pulmonary edema, hypoxemia, and respiratory failure. An essential cause of ALI is blood–gas-barrier breakdown where endothelial cells and type I and II pneumocytes are damaged. During this process, lung edema, as characterized by intravascular fluid leakage into the alveolar sacs, can occur. The loss of type I epithelial integrity and pneumocyte type II destruction decrease the removal of

alveolar fluid, worsening atelectasis and gas exchange.[7] Interestingly, although type II pneumocytes are responsible for lung resolution, their proliferation is not frequently found in ALI.[8] Additionally, with malaria-associated ARDS patients, there are no evidence of pneumocyte type II expansion or restoration in the affected lungs.[9] Therefore, the pathogenesis of malaria-associated ARDS in relation to type II pneumocytic apoptosis leading to lung resolving retardation needs to be additionally explored.

In a recent study, we revealed that hemozoin (HZ), a metabolite from parasitic digestion of hemoglobin in the erythrocyte, directly damages type II pneumocytes and causes cellular apoptosis. A positive correlation between the occurrence of ARDS and the degree of HZ deposition in the lungs was found in the patients with severe malaria.[9] Moreover, HZ can induce cellular destruction by activating monocytes and macrophages to produce several cytokines, but interleukin (IL)-1β especially[10] which is commonly identified in severe malaria cases.[11] Along these lines of thought, the present study aimed to examine the effect of HZ in cases where ALI was induced by direct and immunomodulatory effects, focusing on the mechanism involved in type II pneumocyte apoptosis. The experiments involved culturing pneumocytes with HZ, or with IL-1β triggered by HZ and monocytes (HZ-IL-1β). Apoptosis was detected by fluorescent microscope using ethidium bromide/acridine orange (EB/AO) staining and annexin V-FITC/propidium iodide (PI). To verify the occurrence of apoptosis, mRNA expression of *CARD9* and IL-1β was investigated by quantitative reverse transcription polymerase chain reaction (qRT-PCRs). Moreover, junctional integrity of the basolateral adherens junction in the pneumocytes was investigated using immunohistochemistry with anti-human E-cadherin, a calcium-dependent cellular proliferation and cell division marker.[12] In addition, ultrastructural changes in the pneumocytes were examined using scanning electron microscopy (SEM) and transmission electron microscopy (TEM). Our findings augment current understanding of the host–parasite relationship, in terms of the dysfunction in ALI induced by HZ, whereby the resolution of lung epithelial damage is inhibited in malaria-associated ARDS.

Materials and methods

Cell lines

In vitro co-culture model in this study was conducted with two cell types: lung epithelial cells (pneumocyte type II; A549) and mononuclear cells (THP-1) both of which were obtained from American Type Culture (ATCC), USA. The human lung A549 cell (ATCC-CCL-185) is adenocarcinomic human alveolar basal epithelial cells. In nature, 80–90% of these cells are type II pneumocytes responsible for surfactant production and respiratory resolution, whereas 10–20% of them are type I pneumocytes responsible for gas exchange and diffusion of some substances, such as water and electrolytes, across the alveoli of the lungs. The human THP-1 cell line (ATCC-TIB-202) is a human leukemia monocytic cell, which resembles to primary monocytes and macrophages in its morphology and differentiation properties. To characterize the damage caused to lung epithelial cells or pneumocytes by HZ, *in vitro* co-culture of lung epithelium cells with HZ or HZ-IL-1β was conducted.

Cell cultures

A549 and THP-1 cells were maintained in RPMI-1640 complete medium supplemented with 10% inactivated fetal bovine serum and 1% penicillin/streptomycin (100 U/100 mg/ml). Cells were maintained at 37°C in 5% CO_2 atmosphere. The medium was changed every two to three days.

IL-1β triggered by HZ and monocytes (HZ-IL-1β). THP-1 cells at 1 $\times 10^4$ cells/ml were seeded onto 12 well plates, 2 ml of complete RPMI-1640 medium was added and the cells were exposed to 20 μM HZ for 24 h. The co-cultured cells were centrifuged (1500 r/min, 4°C for 5 min), and the supernatant was collected and kept at −20°C with freeze–thaw avoidance until the experiments were performed.

Direct and immunomodulatic effects of HZ in human lung epithelial cells. For each experiment, 1 $\times 10^4$ A549 cells/ml were seeded with complete RPMI-1640 medium as follows: (i) for TEM, the cells were seeded onto transwell permeable supports (0.4 μm pore-size, 6.5 mm diameter; Costar, Corning Inc., NY, USA), (ii) for light and SEM, the cells were seeded onto plastic cover slips (13 mm diameter; Thermanox, NY, USA), or (iii) for apoptotic staining, the cells were seeded onto 12-well plates (Costar, Corning Inc., NY, USA). The direct effects of HZ on the pneumocyte cells were examined by exposing the cells to 20 μM of HZ for 1, 6, 12, 24, and 48 h. This concentration of HZ was verified to establish an appropriate magnitude of apoptosis before use. To determine the immunomodulatory effects of HZ, the cells were exposed to HZ-IL-1β for the above-mentioned incubation periods. Camptothecin (CPT) (4 μM)[13] was used as a concurrent positive control and complete RPMI-1640 medium was used as a negative control.

Apoptosis detection

EB/AO staining. The numbers and morphologies of apoptotic cells were examined by dual staining with EB/AO. EB is only taken up by cells when the integrity of the cytoplasmic membrane is lost, after which the nucleus will be stained red. Acridine orange (AO) permeates all cells, making nuclei appear green. At each time point, A549 cells were stained. This involved taking the 10^4 cells per ml collected by trypsinization with 0.25% Trypsin-EDTA and washing them with phosphate-buffered saline (PBS). The cells were centrifuged and the supernatant was removed. The cell pellet was re-suspended in 50 μl of complete culture medium. A 10 μl aliquot of 100 μg/ml EB/AO mixture was added to 20 μl of the cell suspension. Cellular morphology and apoptotic cell numbers were examined by fluorescence microscopy.[14]

Detection of apoptotic cells by annexin V-FITC and propidium iodide staining. To verify the results of EB/AO staining of apoptotic cells, annexin V-FITC and PI staining were used. Phosphatidyl serine externalization is indicative of early stage apoptosis, and therefore, apoptotic cells were quantified using the FITC Annexin V-propidium iodide apoptosis detection kit (ImmunoTools, Friesoythe, Germany). At various interval times, the cultured A549 cells were harvested by trypsinization with 0.25% Trypsin-EDTA. The cells were centrifuged and then washed in 0.1 M PBS. The pellet was resuspended in 90 µl of annexin V binding buffer (diluted 1:1), and then stained with 5 µl of FITC-conjugated Annexin V (diluted 1:10) and 5 µl of PI solution for 20 min in the dark. Finally, 400 µl of binding buffer was added with gentle mixing and the solution was kept on ice before immediate examination by fluorescence microscopy.[15]

Interpretation of apoptotic cell staining

EB/AO staining. The apoptotic staining pattern of EB/AO was differentiated according to the following criteria: normal cells, green with regular nuclei; early apoptotic cells, yellow to green with fragmented nuclei or condensed chromatin; late apoptotic cells, orange to red with fragmented nuclei; necrotic cells, red with pyknotic nuclei.[14,16]

AnnexinV-FITC PI staining. The annexin V-FITC/PI staining pattern categories of the apoptotic cells were determined as follows: Green coloration represents early apoptotic cells, green and red coloration represents late apoptotic cells, red coloration from PI in the nucleus represents necrotic cells, and normal cells with regular membrane integrity were not stained by annexin V/FITC or PI.[15]

Scanning electron microscope. Selected A549 cells on cover slip were washed with 0.1 M sucrose phosphate buffer (SPB), fixed with 2.5% glutaraldehyde in 0.1 M SPB, pH 7.4 for 1 h, and then washed with the same buffer for three times, for 10 min. After air-drying, the specimens were placed on aluminum stubs, coated with gold in gold sputter machine (model K550, Emitech Ltd, Kent, England), and examined under SEM (model JSM-6610LV, JEOL, Tokyo, Japan).

Transmission electron microscope. To characterize internal fine morphology resulting from HZ-induced ALI, the selected A549 cells on a transwell membrane were washed twice in PBS, and fixed with 2.5% glutaraldehyde in 0.1 M SPB for 1 h.[17] The cells were then subjected to post-fixation with 1% osmium tetroxide for 1 h and then washed at least three times with 0.1 M SPB. The cells were dehydrated with a graded ethanol series (30%, 50%, and 70%; 10 min each). Infiltration was achieved using LR white resin with 70% ethanol (1:1 and 2:1) for 30 min each at room temperature followed by 100% LR at 4°C for overnight. The membrane was transferred to absolute LR white in a beam capsule to avoid exposure to air. The capsules were incubated in a 60°C oven for 48 h and the samples were cut into ultrathin sections (90 nm) using an ultramicrotome. The ultrathin sections were post-stained with uranyl acetate for 1 min (light exposure was avoided), lead citrate was added for 3 min (CO_2 exposure was avoided) followed by washing in CO_2-free water. The samples were stored in desiccators until examination by TEM (model HT7700–6610LV, Hitachi, Tokyo, Japan).

Quantitative reverse transcriptase polymerase chain reaction. To investigate the role of apoptotic genes and cytokine gene expression in HZ-induced ALI, the expression levels of *CARD9* and IL-1β genes were measured in the pneumocytes. RNA was isolated with TRIZOL reagent (Invitrogen, MA, USA). Reverse transcription of the mRNA to generate cDNA and qRT-PCR was conducted using the KAPA SYBR FAST One-Step qRT-PCR Kit (KAPA BIOSYSTEMS, Californai, USA). The *CARD9* primer sequences were 5′-TCCGACCTGGAAGA TGGCTCAC-3′ (forward primer) and 5′-CAGAGCTGC AAAGGGCTGTTTC-3′ (reverse primer). The IL-1β primer sequences were 5′-ACAGATGAAGTGCTCCTTCCA-3′ (forward primer) and 5′-CAGAGCTGCAAAGGGCT GTTTC-3′ (reverse primer). The β-actin mRNA expression level was used for normalization with 5′-GGCCAGGT CATCACCATT-3′ and 5′-GTCGGAGATTCGTAGCTGGAT-3′ forward and reverse primers, respectively. qRT-PCR was performed using the CFX96 Touch™ Real-time PCR detection system thermocycler and the relative mRNA levels were calculated using the $2^{-\Delta\Delta C}{}_T$ method.[18,19]

Immunohistochemistry. To identify junctional defects in HZ-induced ALI, A549 cells on cover slips were washed in PBS twice, fixed with 4% paraformaldehyde in PBS for 15 min, and then washed in wash buffer (EnVision™ FLEX, DAKO, USA) twice. The cells were permeabilized with 1% Triton-X 100 in PBS for 30 min on ice, washed three times, and incubated with EnVision™ FLEX peroxidase-blocking reagent (DAKO, USA) for 10 min at room temperature. Purified mouse anti-human E-cadherin (BioLegend, San Diego, CA, USA) was added to the cells for 1 h at room temperature. The cells were then washed and EnVision™ FLEX/HRP (DAKO, USA) was added for 1 h. After rewashing, the cells were incubated in 3′-diaminobenzidine (DAB, DAKO, USA) for 5 min. The DAB reaction was stopped by washing in tap water for 10 min. The cells were then counterstained with hematoxylin for 15–30 s, mounted, and then examined by light microscopy. To determine whether junctional alteration occurs during HZ- and HZ-IL-1β-induced apoptosis, at least 10 medium power fields (10×)/group were examined to determine the degree of intensity score multiplication and the area of expression (H-scores), following the method used in our previous study.[9,20] Briefly, the intensity score was graded into three levels: 0 for no staining, +1 for low-intensity staining, +2 for medium-intensity staining, and +3 for high-intensity staining. The expression area was determined using an image analysis program (ImageJ® Version 1.36; NIH, USA). The color images obtained were transformed to gray scale, the labeling area was located using the threshold mode, and the

values obtained were calculated as the percentage expression.

Immunogold labeling of LC-3 (microtubule-associated protein 1 light chain 3). The ultrathin sections were incubated in 50 mM glycine in PBS (pH 7.4). Non-specific binding in the sections was blocked with 5% bovine serum albumin (BSA) (25557, EMS, USA) pH 7.4. The sections were washed with incubation buffer (0.1% BSA in PBS) followed by incubation in rabbit polyclonal anti-LC3 antibody (MyBioSource, San Diego, USA) for 1 h. The sections were incubated in goat anti-rabbit IgG conjugated with 5 nm gold particles (G7402, Sigma Aldrich, Germany). Afterwards, the sections were washed with incubation buffer and distilled water for 1 h, and then treated with the Aurion R-Gent SE-EM kit, 25521 silver enhancement kit (EMS, USA) to enhance the gold signaling. The sections were post-stained with uranyl acetate for 1 min, lead citrate for 3 min and then washed in CO_2-free water. The samples were stored in desiccators until TEM was performed.

Statistical analysis. All the data presented herein are the mean ± standard error of mean and the analysis used PASW® Statistics version 18.0 software (SPSS Inc., Chicago, USA). Kolmogorov–Smirnov Goodness of fit was used to test the data distribution of all the quantitative parameters such as apoptotic scores, cell numbers, percentage of positive cells, H-score and relative mRNA expression levels. ANOVA and correlation tests were used to differentiate the differences between the groups in this study. Curve estimation was used to evaluate the apoptosis levels over time. Statistical significant was determined at P-values of ≤ 0.05.

Results

Determining the concentration of HZ required to induce apoptosis

The HZ dosage was determined before use. Apoptotic pneumocytes were characterized by cytoplasmic blebing and hyperchromatic nucleus as shown in Figure 1. With A549 cells, HZ concentrations of 2, 5, and 10 μM were not appeared an enough number of apoptotic cells, with 20 μM of HZ being more effective. However, at a 100 μM concentration, HZ induced excessive cellular apoptosis. Consequently, the cells were exposed to HZ at 20 μM because this was the minimum concentration capable of initiating visually obvious apoptosis.

HZ can induce apoptosis in A549 cells by direct and immunomodulatory effects

The direct and immunomodulatory effects of HZ on A549 cells were determined by examining cellular apoptosis. After A549 cells were exposed to HZ and HZ-IL-1β, apoptosis was evaluated using EB/AO, Annexin V-FITC/PI, and ultrastructural studies.

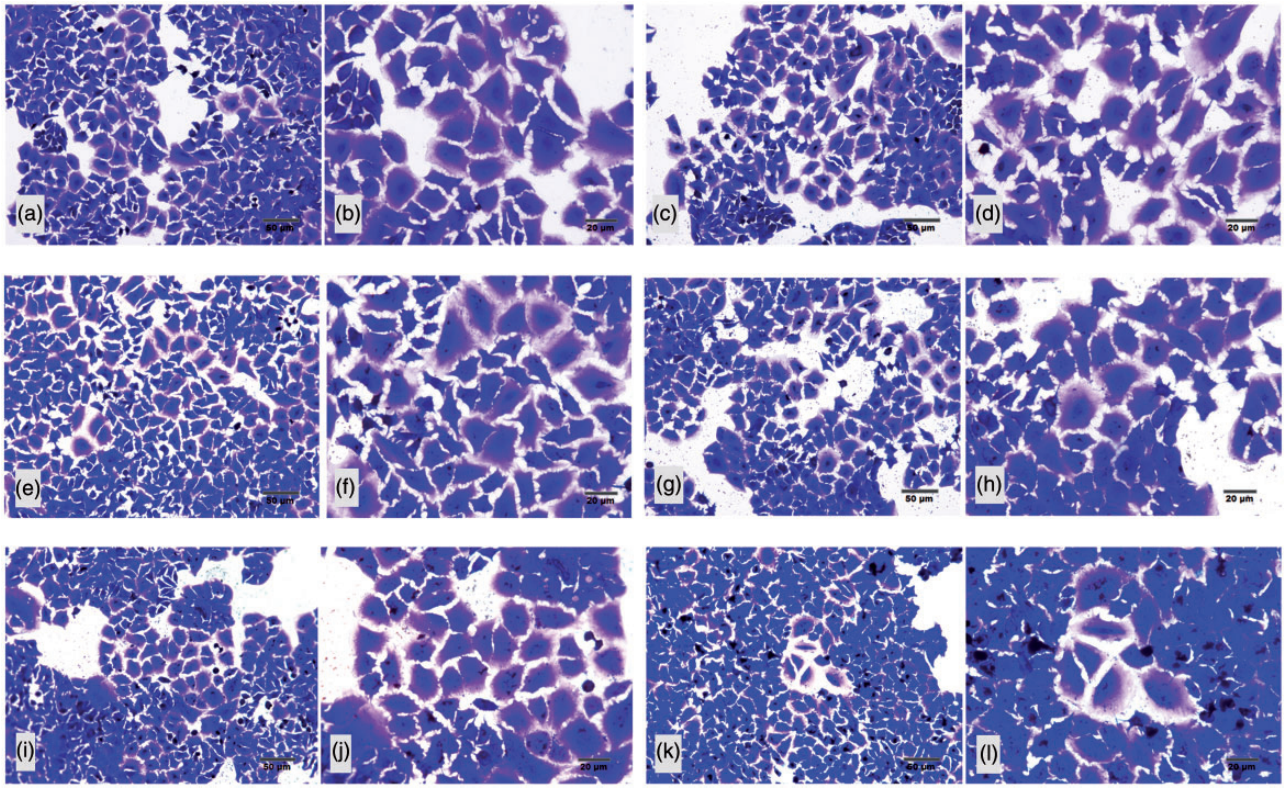

Figure 1. Morphology of A549 apoptotic cells at five difference concentrations of HZ. The appropriate dose of HZ capable of inducing apoptosis in A549 cells was established by culturing the cells in the following concentrations of HZ: (a) 0 μM (negative control), (b) 2 μM, (c) 5 μM, (d) 10 μM, (e) 20 μM, and (f) 100 μM. Post induction, the intact cells showed large and cuboidal flattening and blue staining, whereas the apoptotic cells were small and starry like with hyperchromatic or dark nuclei. (A color version of this figure is available in the online journal.)

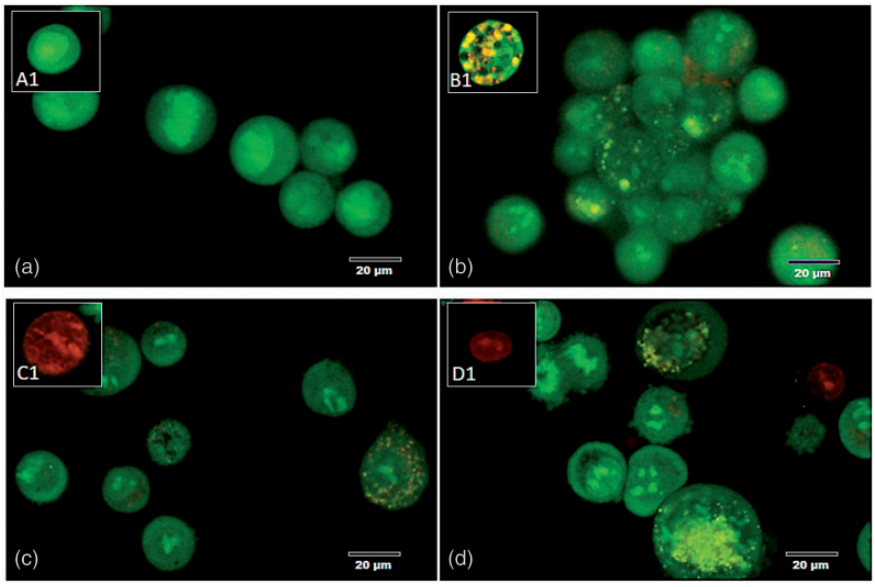

Figure 2. Morphology and EB/AO staining pattern of apoptotic cells. (a) A normal pneumocyte from the non-treated group with a green-stained appearance and intact nucleus. (b–d) The appearance of the apoptotic pneumocytes showed green to yellow staining with fragmented nuclei in the (b) CPT, (c) HZ, and (d) HZ-IL-1β treatment groups. (A color version of this figure is available in the online journal.)

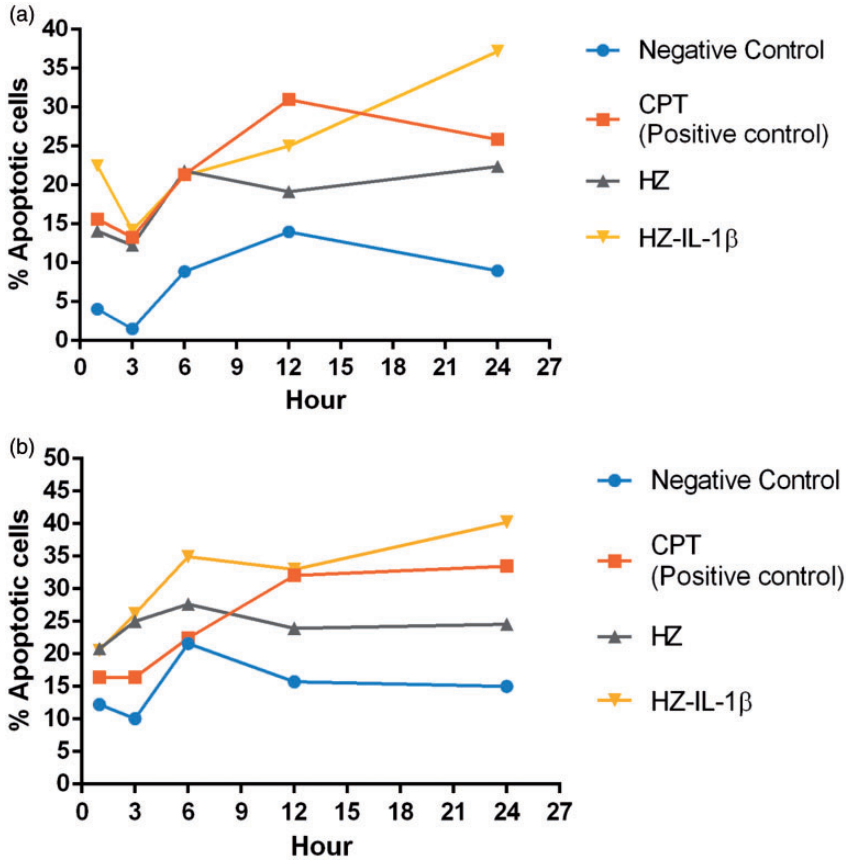

Figure 3. Percentage of apoptotic pneumocytes treated with HZ. The number of apoptotic cells from EB/AO and annexin V-FITC/PI staining was calculated from line graphs. (a, b) At 1 h post-exposure, the group with the fastest cellular apoptotic induction was HZ-IL-1β. CPT and HZ alone groups were the next to reach high apoptosis levels after 6 and 12 h exposure times. At 24 h post-exposure, the HZ-IL-1β groups had higher numbers of apoptotic cells than those of the CPT-, HZ- and no-treatment groups. (A color version of this figure is available in the online journal.)

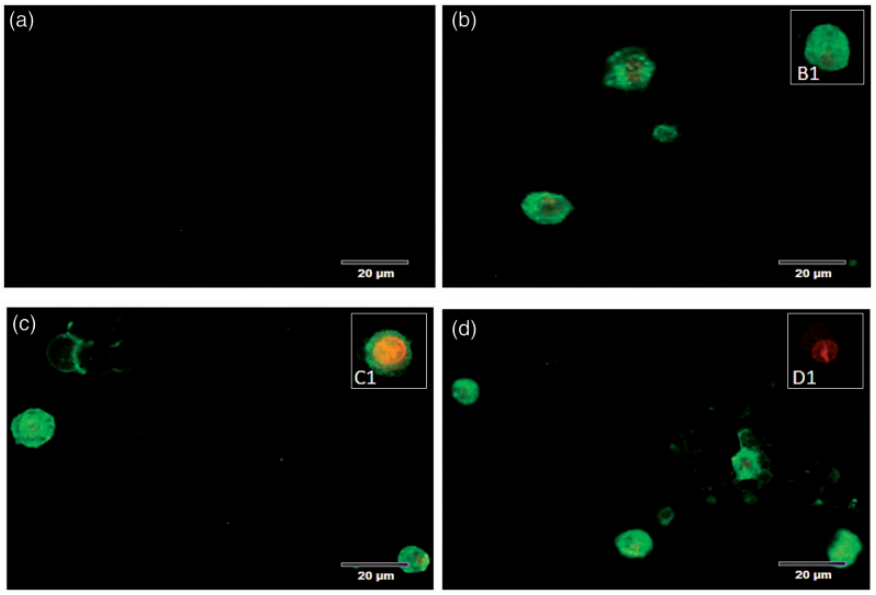

Figure 4. Morphology and annexin V-FITC/PI staining pattern of apoptotic cells. (a) In the no-treatment group, the intact pneumocytes were neither stained with annexin V-FITC nor PI, whereas the apoptotic pneumocytes were stained with annexin V-FITC with or without PI as shown in (b) CPT, (c) HZ, and (d) HZ with the THP-1 supernatant-treated group. (A color version of this figure is available in the online journal.)

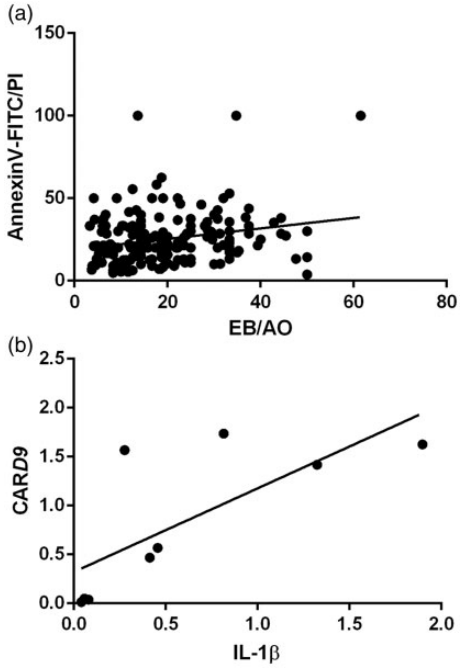

Figure 5. Positive correlation between the apoptotic cell numbers determined by the different stains and IL-1β and *CARD9* gene expression.

Table 1. The occurrence of apoptosis in type II pneumocyte during exposed with any treatment represented by cubic shaped as determined R^2 and *P*-value from curve estimation.

	EB/AO		*Annexin V-FITC/PI*	
	R^2	*P*	R^2	*P*
NEG	0.270	0.002	0.228	0.007
CPT	0.413	0.000	0.551	0.000
HZ	0.113	0.135	0.292	0.001
HZ-IL-1β	0.264	0.003	0.122	0.110

EB/AO staining

The HZ-IL-1β-treated cells had higher levels of apoptosis than the cells treated with HZ alone. The effects of HZ exposure in the A549 cells were also investigated over time. Treated cells were differentiated by green colorization with regular nuclei (normal) (Figure 2(a1)), yellow to green colorization with fragmented nuclei or condensed chromatin (early apoptotic cell) (Figure 2(b1)), orange to red colorization with fragmented nuclei (late apoptotic cell) (Figure2 (c1)), whereas necrotic cells were red in color with pyknotic nuclei (Figure 2(d1)). After the A549 cells were treated with HZ-IL-1β for 1 h, apoptosis occurred rapidly unlike the A549 cells treated with HZ or CPT. After 6 to 12 h exposure to HZ or CPT, the numbers of apoptotic A549 cells increased, while the cells treated with HZ-IL-1β for 24 h had the highest numbers compared with the CPT- and HZ-treated groups (Figure 3(a)).

AnnexinV-FITC/PI staining

Annexin V and PI staining claimed that when A549 cells exposed to HZ, HZ-IL-1β, and CPT, they highly presented an early apoptosis during first 24 h when compared to non-treated group. However, no significant differences were observed among the treatment groups. Additionally, HZ with HZ-IL-1β treatment tended to induce higher levels of apoptosis than that observed with CPT or HZ alone, as compared with the no treatment group (Figure 3(b)). The stages of cellular apoptosis were differentiated by their coloration; green stained early apoptotic cells (Figure 3(b1)) and green via red stained late apoptotic cells (Figure 4 (c1)). The cells with only red stained nuclei were necrotic cells (Figure 4(d1)), whereas normal cells with regular membrane integrity were not strained after annexin

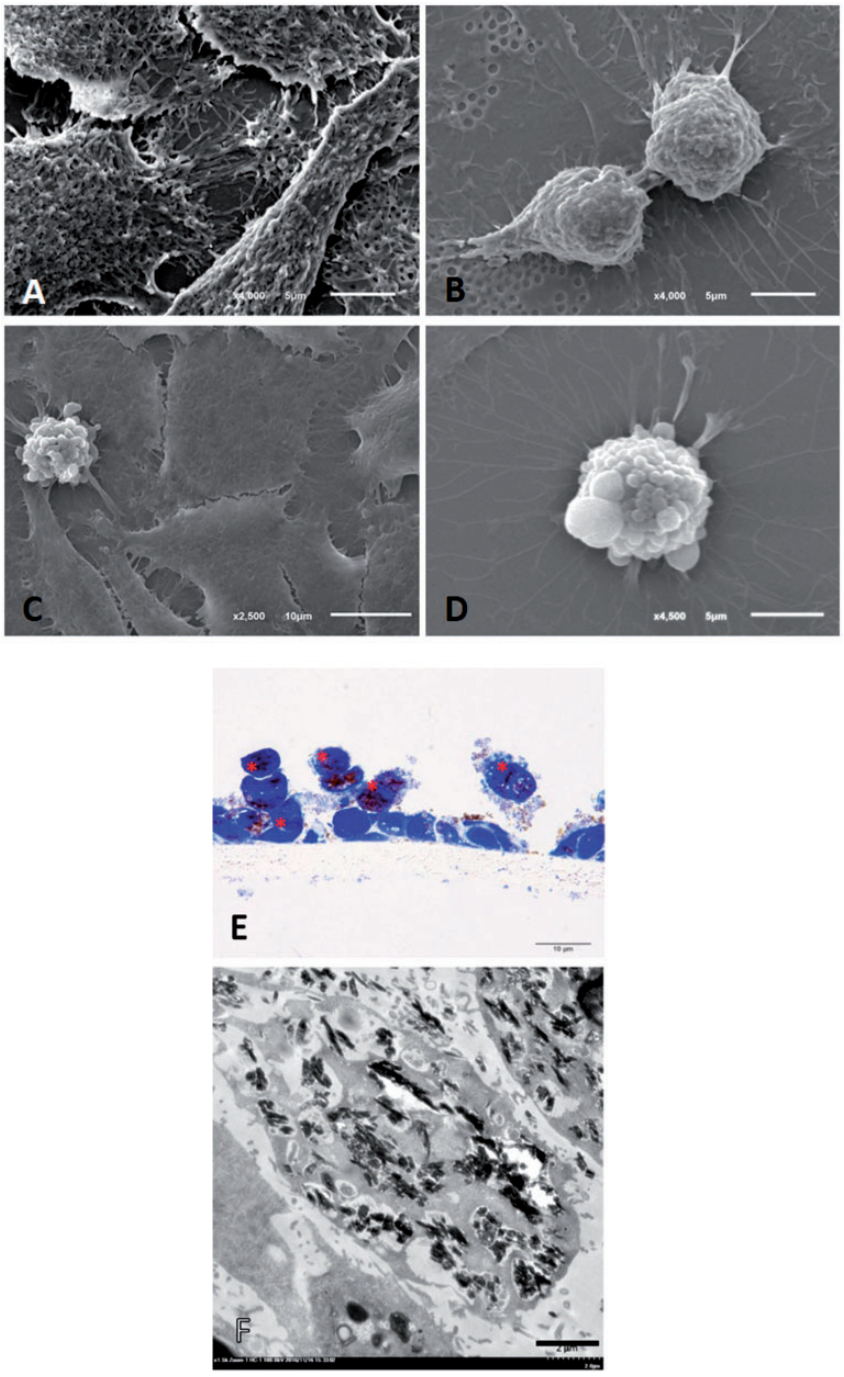

Figure 6. Fine morphological structure of A549 cells with or without apoptosis. The electron micrographs showed that (a) mature A549 cells were generally flat with irregular surfaces; (b) A549 progenitor cells were round with regular or irregular surfaces; (c, d) apoptotic A549 cells had blebs on their surfaces. (e) Semi-thin section of A549 cells with toluidine blue staining showing the HZ-treated apoptotic cells (*). HZ pigment deposited in the pneumocytes was frequently found in the HZ and HZ-IL-1β treatment groups (f). (A color version of this figure is available in the online journal.)

V/FITC or PI treatment (Figure 4(a1)). Interestingly, there was a positive correlation between a number of apoptotic cells from EB/AO and Annexin V-FITC/PI staining techniques (Spearman's rho correlation = 0.315, $P = 0.000$) (Figure 5(a)).

The results of the EB/AO and annexin V-FITC/PI staining tests to detect apoptosis enabled us to predict the trend underlying apoptosis in the A549 cells (with or without treatment), via estimation curves. Almost all the curves had cubic-shaped correlations and had the highest r^2 values when compared with curves of other shapes and also had significant P-values, as shown in Table 1.

Scanning electron microscopic study

SEM was performed to examine the external surfaces of the apoptotic cells in three dimensions after HZ, CPT, or HZ-IL-1β treatment. The apoptotic cells in all the treatment

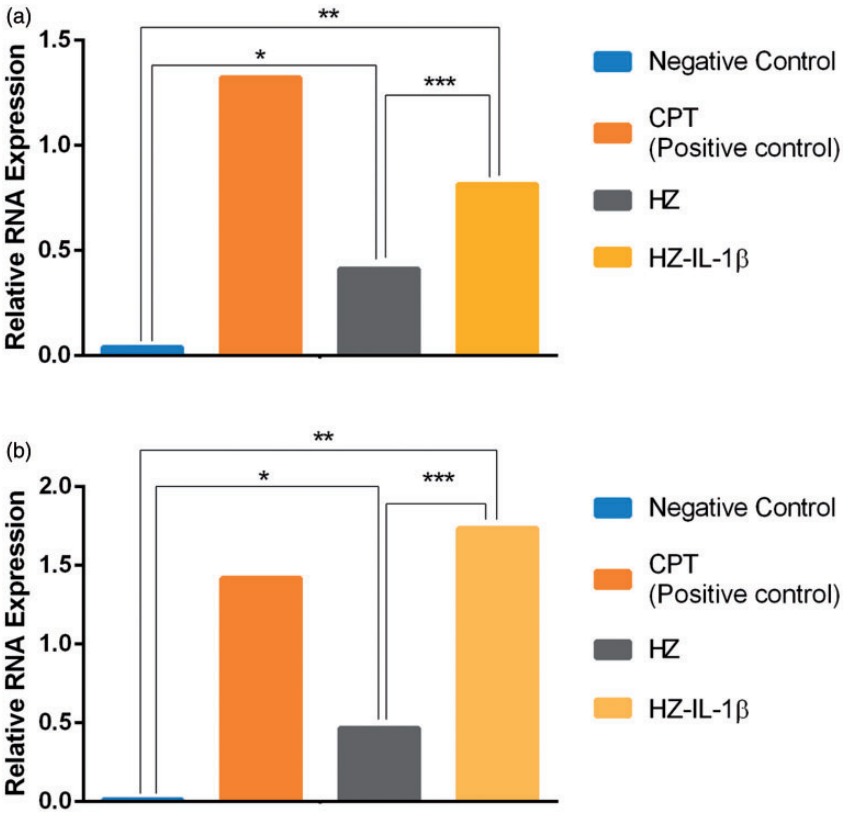

Figure 7. IL-1β and CARD9 mRNA expression in A549 cells by treatment group. HZ was able to up-regulate IL-1β and *CARD9* levels in A549 cells. (a, b) HZ was able to induce apoptosis by its immunomodulatory activity but not in the non-treated group. CPT was the most effective treatment at inducing IL-1β genes (a), while HZ-IL-1β was the most effective treatment at inducing *CARD9* gene expression (b). (A color version of this figure is available in the online journal.)

groups showed membrane blebbing, unlike the non-apoptotic pneumocytes, which had intact membranes (Figure 6(a) to (d)).

Transmission electron microscopic study

TEM was performed to examine the intracellular morphologies of the apoptotic cells when destroyed by exposure to HZ, CPT, or HZ-IL-1β. The ultrastructural changes in the A549 cells treated with HZ for 24 h are shown in Figure 6(e) and (f), which mainly presents as an accumulation of HZ in the apoptotic type II pneumocytes.

HZ treatment upregulated the levels of IL-1β and *CARD9*

It is well established that A549 cells are activated by foreign bodies to produce IL-1β and *CARD9*.[21,22] Therefore, the IL-1β and *CARD9* transcript levels in these cells were investigated using qRT-PCR. The results showed that expression of IL-1β and *CARD9* mRNAs was higher in the A549 cells treated with HZ and HZ-IL-1β than in the non-treated group. Interestingly, HZ-IL-1β and CPT both induced the highest expression of these two genes when compared to HZ alone or the non-treatment group (Figure 7). In addition, a positive correlation between IL-1β and *CARD9* gene expression was noted (Spearman's rho correlation = 0.817, $P = 0.007$) (Figure 5(b)).

HZ is capable of suppressing E-cadherin function

E-cadherin protein is located basolaterally between the cells in adherens junctions, especially in epithelial cells. This protein is responsible for the integrity of the airway barrier and is capable of preventing environmental substances accessing the submucosal regions of the airways.[12,23] To characterize the effect of HZ on the A549 cells, we immunohistochemically stained this junctional marker in pneumocyte cells. Figure 8(a) to (d) shows an E-cadherin immunolabeled junction between the cell-to-cell interfaces. The results also revealed that E-cadherin expression was down regulated in all the treatment groups except in the non-treated control group (Figure 8(e)). We also found that the HZ-IL-1β-treated group had the most suppressed level of E-cadherin expression.

Lipid surfactant in multivesicular bodies was substituted for HZ in A549 cells to induce apoptosis

It has been established that the pulmonary surfactant produced by type II pneumocytes is deposited in MBs,[24] but several factors affect its production and secretion. Interestingly, our electron microscopic studies revealed that HZ accumulated in the MBs in the HZ-treated apoptotic A549 cells (Figure 9). The A549 cells co-cultured with HZ presented as apoptotic pneumocytes, as indicated by the presence of disintegrated cytoplasm and accompanying HZ accumulation. To investigate the autophagic activity of type II pneumocytes during apoptosis, LC-3

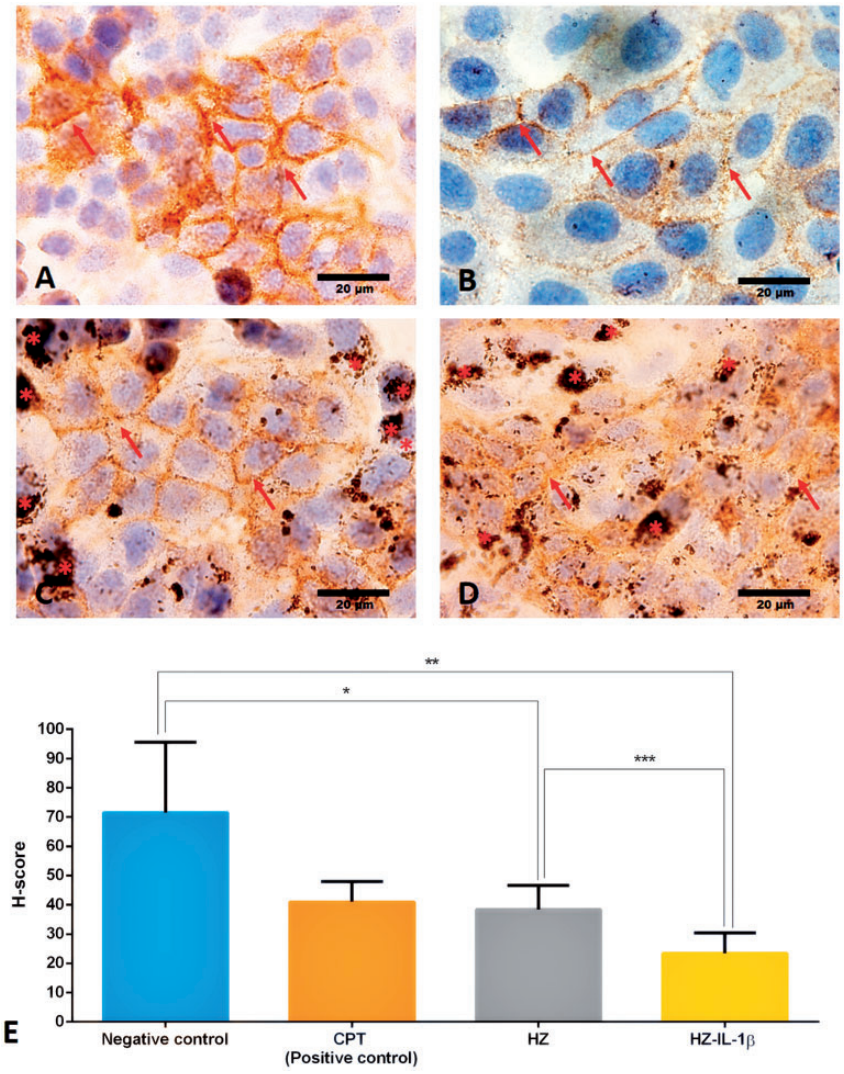

Figure 8. Immunohistochemical staining of E-cadherin in A549 cells by treatment group. A549 cells co-cultured with HZ or HZ-IL-1β were able to suppress E-cadherin expression. (a) Cells in the no-treatment group had intensive brown staining (arrow), whereas the groups treated with (b) CPT, (c) HZ, or (d) HZ-IL-1β rarely showed DAB staining accompanying HZ accumulation (*). (e) H-scores were calculated from the percentage of an area of expression/high power field and the intensity score. The results show that all the treatment groups experienced down-regulated E-cadherin expression. The HZ-IL-1β treatment group had the most pronounced suppression of E-cadherin expression in the pneumocytes, and the CPT and HZ treatment groups less so when compared with the no treatment group. (A color version of this figure is available in the online journal.)

immunogold labeling was conducted. The results showed that pneumocytes with HZ deposition had higher levels of LC-3 labeling than intact pneumocytes (Figure 10).

Discussion

Lung alternations in falciparum malaria include airflow obstruction, impaired ventilation, reduced gas transfer, and increased respiratory phagocytic activity.[25] The worsening or persistence of these gas exchange abnormalities after treatment and beyond the expected time of parasitized clearance reflects a prolonged inflammatory response and the genesis of ALI. In animal studies, once in the circulation, HZ is rapidly taken up by circulating mononuclear cells and tissue macrophages in relevant to the production of pro-inflammatory mediators, such as IL-1β and tumor necrotic factor (TNF)-α .[26] HZ itself also induces a strong alveolar inflammatory response and contains pro-oxidative property.[27] Regarding to the capacity of HZ, it triggers the innate immune response and inflammatory signaling pathways.[28] In addition, several pathological changes for instance alveolar thickening membrane, fluid deposition in alveolar sac, hyaline membrane formation, HZ pigment ladened macrophage, and parasitized erythrocytes with endothelial cells damage are found in patients with malaria-associated ARDS.[9] Notably, the lungs of patients with ARDS have high HZ pigment deposition when compared with non-ARDS patients and intact lungs. All of these occurrences indicate an important role of HZ to the severity and pathogenicity of ALI in severe malaria pathogenesis.

In this study, the effect of HZ on pneumocyte type II during ALI, focusing on the lung resolution was conducted. The results revealed that HZ modulated pnuemocytic apoptosis in association with both direct and immunomodulatic effects. The immunomodulatory effect

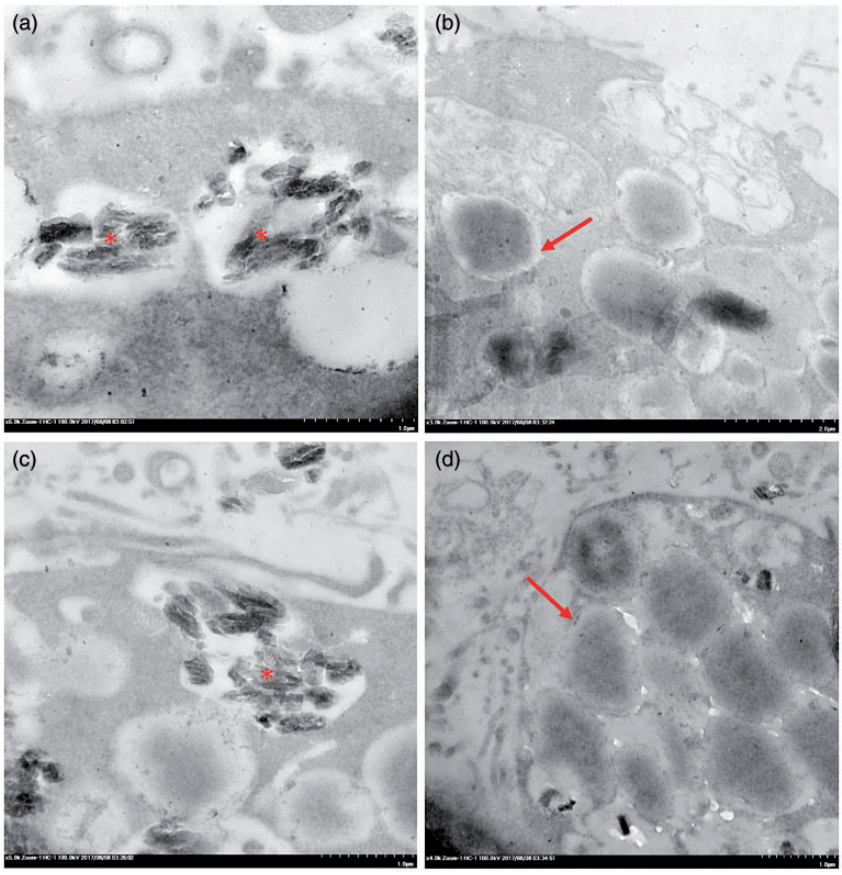

Figure 9. Transmission electron micrograph of multivesicular bodies in pneumocytes exposed to HZ. Accumulation of HZ (*) showing lipid substitution in the multivesicular bodies (arrow).

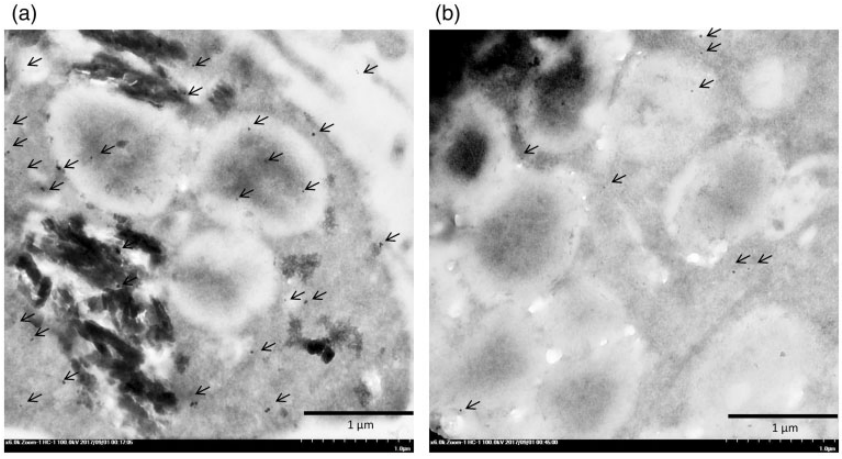

Figure 10. Immunogold labeling of LC-3 in the surfactant vesicles. A number of LC-3 labeled gold particles (arrow) were found in the HZ-pigment-laden pneumocytes (a) as compared with the intact type II pneumocytes (b).

was characterized by the triggering of mononuclear cells to produce IL-1β, which led to apoptosis as shown by apoptotic staining, apoptotic gene expression (*CARD9*), and a junctional defect via down-regulation of E-cadherin and the subsequent loss of alveolar integrity and impediment of lung resolution (Figure 11). It is well described that apoptosis in lung epithelial cell is a potentially important factor contributing to the loss of pneumocyte cells subsequent to the development of ALI in infancy.[29] Furthermore, various apoptotic markers are used to be candidate for cellular apoptosis detection in ALI. For example, caspase-cleaved cytokeratin-18 increases in bronchoalveolar lavage fluid during ALI.[30] Caspase-3, Bax, and p53 are also increased in the lungs from patients who died with ALI.[31] Moreover, the apoptosis regulator gene *CARD9* is also involved in the apoptotic pathway and interacts with BCL-10 to

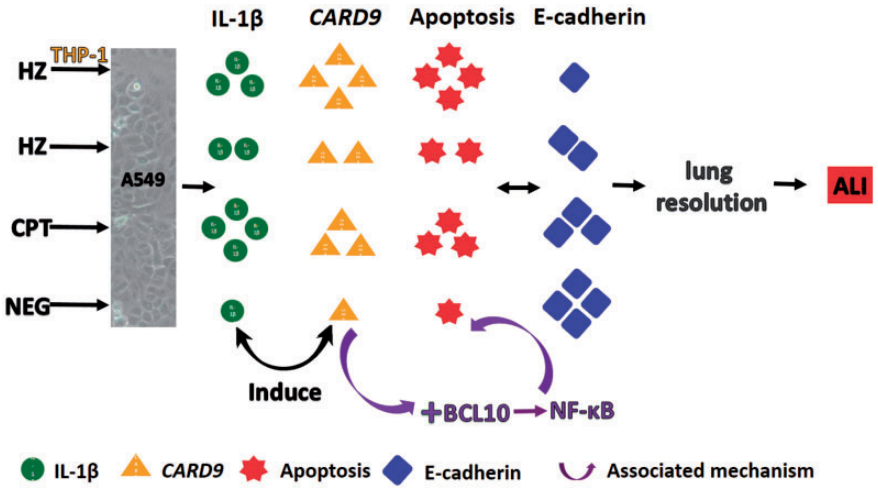

Figure 11. Possible mechanism for the retardation of lung resolution in HZ-induced ALI in relation to IL-1β and *CARD9* regulation. (A color version of this figure is available in the online journal.)

regulate nuclear factor-kappa B (NF-κB)[18,32] to signal the innate immune response in the lungs.[33] Therefore, it is point out that NF-κB is an important regulator for ALI cooperating to the role of IL-1β and *CARD9*. Interestingly, it has been reported that NF-κB is a crucial factor that modulates apoptosis in the brain, kidney, and liver during severe malaria.[34–36] The relationship between apoptosis and its regulatory factors (e.g., *CARD9*, BCL-10, and NF-κB) suggests that the *CARD9* pathway may be involved in type II pneumocyte apoptosis and plays an important role in ALI during severe malaria, and also be an aggravating factor that retards alveolar restoration.

Not only immunomodulatic effect of HZ that contributes to apoptosis or cellular destruction, the physical property based on its characteristic and morphology is an additional considered factors. Actually, HZ crystal leads to permanent destruction of the cells and their functions.[37,38] The ultrastructural studies reported herein on HZ have revealed that its crystal-like structure and shape with sharp edges (Figures 6 and 9) can directly irritate cells and result in cellular damage. In fact it has already been reported that differences in the size and shape of HZ are implicated in the severity of cell injury, in terms of cellular biochemical and morphological interference.[39]

Lung epithelial injury and apoptosis are critical factors underlying the mechanism of damage in ALI.[40,41] Therefore, this study exploited the different staining patterns of EB/AO and annexin V-FITC/PI to investigate apoptosis in pneumocytes treated with HZ Figures 2 and 4. EB/AO stained nucleus, whereas AnnexinV-FITC/PI stained membrane and cytoplasm.[42] The Annexin conjugated with FITC was stuck into phosphatidylserine which is located on the membrane and flipped out during cellular apoptosis. Moreover, the apoptotic cells in advance stage were dramatically membrane destroyed, PI was able to directly penetrate through the nucleus.[43] Interestingly, regarding to our results (Figure 5), there was a positive correlation between a number of apoptotic pneumocyte using EB/AO and Annexin V-FITC staining. This correlation confirmed the validity of the obtained results in this study.

During malaria-associated ARDS, which is the severest form of ALI, breakdown of the blood–gas-barrier causes a deterioration in the endothelial–epithelial and epithelial–epithelial cell layers.[44] Therefore, cellular detachment or junctional defects are important factors to be considered in this context. In this study, E-cadherin, which is found in the basolateral adherens junctions generally located on epithelial cells, was selected as a marker to determine the effect of HZ-induced junctional alteration. Subsequently, our results showed that when A549 cells are exposed to HZ and HZ-IL-1β, E-cadherin expression was suppressed (Figure 8), leading to cellular interaction losses. It is clear that junctional defects have a negative effect on cell viability and cause imbalance of cellular homeostasis.[45] Moreover, effective alveolar epithelium restoration hinges on appropriate coordination between rearrangement and reformation of a functional barrier, and several factors are involved in this process, especially E-cadherin protein, extracellular matrix turnover, and reestablishment of type II pneumocytes.[46] Regarding to our results, alveolar epithelial restoration was impeded subsequent to type II pneumocyte apoptosis and losing of cell-to-cell interaction characterized by down-regulation of E-cadherin.

Furthermore, our ultrastructural study revealed that an important morphological change had occurred in the apoptotic type II pneumocytes: membrane blebbing (Figure 6). Of note, the transmission electron micrographs showed that the cytoplasm had disintegrated in the apoptotic type II pneumocytes, and that HZ was deposited in the surfactant vesicles that generally contain lipid material, as represented by multivesicular bodies (MBs) (Figure 9). It is assumed that HZ dissolves completely in the lipids within the parasite's digestive vacuole, which is a necessary requirement for its crystallization and production.[47] *In vivo* study indicated that HZ alters the lipid composition of the surfactant from phosphatidylcholine and esterified cholesterol to lysophosphatidylcholine, which possibly contributes to malaria-associated ARDS.[48] In accordance with

our study, replacing HZ in the vesicles provided additional evidence to support the interfered role of HZ in alveolar surfactant alteration, which is central feature of the pathogenesis of ALI. However, the reason(s) why HZ is observed in lipid vesicles requires further investigation. We also conducted immunogold labeling of LC3, a marker of modulatory autophagy, in A549 cells and found that apoptotic pneumocytes with HZ deposition had higher LC3 labeling than those without (Figure 10). Moreover, it has been reported that LC3 has a close relationship with all stages of apoptosis, with time-dependency in several diseases (e.g. neurodegenerative diseases)[49,50] and in ALI also.[51] Identifying LC3 labeling in association with HZ accumulation suggests that HZ can induce apoptosis via its direct or immunomodulatory roles. Nevertheless, the role played by HZ in autophagy and apoptosis requires additional studies to uncover the underlying mechanistic details.

In summary, it can be concluded that HZ alone, and HZ with its immunomodulatory effects on immunological cells such as monocytes, was able to induce pneumocyte apoptosis in relation to IL-1β production through the *CARD9* pathway. This occurrence may be a possible pathway for the retardation of lung resolution leading to blood–gas-barrier breakdown, as characterized the by down-regulation of E-cadherin.

Author's contributions: SA, NL, SM, UC and YM participated in the design, interpretation, and analysis of the studies; SM and SA conducted the histopathological, immunohistochemical and electron microscopic studies, NL and SM conducted the *in vitro* co-culture studies and performed real-time RT-PCR. All authors wrote, revised and approved the final manuscript.

DECLARATION OF CONFLICTING INTERESTS

The author(s) declared no potential conflicts of interest with respect to the research, authorship, and/or publication of this article.

FUNDING

This study was supported by Faculty of Tropical Medicine Fund, Fiscal year 2014, Faculty of Tropical Medicine, Mahidol University, Thailand.

REFERENCES

1. Wassmer SC, Grau GE. Severe malaria: what's new on the pathogenesis front? *Int J Parasitol* 2017;**47**:145–52
2. Sein KK, Maeno Y, Thuc HV, Anh TK, Aikawa M. Differential sequestration of parasitized erythrocytes in the cerebrum and cerebellum in human cerebral malaria. *Am J Trop Med Hyg* 1993;**48**:504–11
3. Nguansangiam S, Day NP, Hien TT, Mai NT, Chaisri U, Riganti M, Dondorp AM, Lee SJ, Phu NH, Turner GD, White NJ, Ferguson DJ, Pongponratn E. A quantitative ultrastructural study of renal pathology in fatal Plasmodium falciparum malaria. *Trop Med Int Health* 2007;**12**:1037–50
4. Taylor WR, Hanson J, Turner GD, White NJ, Dondorp AM. Respiratory manifestations of malaria. *Chest* 2012;**142**:492–505
5. Mohan A, Sharma SK, Bollineni S. Acute lung injury and acute respiratory distress syndrome in malaria. *J Vector Borne Dis* 2008;**45**:179–93
6. Johnson ER, Matthay MA. Acute lung injury: epidemiology, pathogenesis, and treatment. *J Aerosol Med Pulm Drug Deliv* 2010;**23**:243–52
7. Luh SP, Chiang CH. Acute lung injury/acute respiratory distress syndrome (ALI/ARDS): the mechanism, present strategies and future perspectives of therapies. *J Zhejiang Univ* 2007;**8**:60–9
8. Stanley MW, Henry-Stanley MJ, Gajl-Peczalska KJ, Bitterman PB. Hyperplasia of type II pneumocytes in acute lung injury. Cytologic findings of sequential bronchoalveolar lavage. *Am J Clin Pathol* 1992;**97**:669–77
9. Maknitikul S, Luplertlop N, Grau GER, Ampawong S. Dysregulation of pulmonary endothelial protein C receptor and thrombomodulin in severe falciparum malaria-associated ARDS relevant to hemozoin. *PLoS One* 2017;**12**:e0181674
10. Kumsiri R, Potup P, Chotivanich K, Petmitr S, Kalambaheti T, Maneerat Y. Blood stage Plasmodium falciparum antigens induce T cell independent immunoglobulin production via B cell activation factor of the TNF family (BAFF) pathway. *Acta Trop* 2010;**116**:217–26
11. Prakash D, Fesel C, Jain R, Cazenave P-A, Mishra GC, Pied S. Clusters of cytokines determine malaria severity in plasmodium falciparum-infected patients from endemic areas of central India. *J Infect Dis* 2006;**194**:198–207
12. Nawijn MC, Hackett TL, Postma DS, van Oosterhout AJ, Heijink IH. E-cadherin: gatekeeper of airway mucosa and allergic sensitization. *Trends Immunol* 2011;**32**:114
13. Ibrahim S, Gao D, Sinko PJ. Selective cytotoxicity and combined effects of camptothecin or paclitaxel with sodium-R-alpha lipoate on A549 human non-small cell lung cancer cells. *Nutr Cancer* 2014;**66**:492–9
14. Ribble D Goldstein NB, Norris DA, Shellman YG. A simple technique for quantifying apoptosis in 96-well plates. *BMC Biotechnol* 2005;**5**:1–7
15. Farha AK, Geetha BS, Nair MS, Dhanya SR, Latha PG, Remani P. Apoptosis mediated cytotoxicity induce by isodeoxyelephantopin on nasopharyngeal carcinoma cells. *Asian J Pharm Clin Res* 2013;**6**:51–6
16. Milena G, Ćurčić MSS, Emina M, Mrkalić, Zoran D, Matović, Dragić D, Banković, Danijela M, Cvetković, Dragana S, Đačić Snežana D. Marković antiproliferative and proapoptotic activities of methanolic extracts from Ligustrum vulgare L. as an individual treatment and in combination with palladium complex. *Int J Mol Sci* 2012;**13**:2521–34
17. Maria Iris Hermanns REU, Kai K, Kirsten P, Charles JK. Lung epithelial cell lines in coculture with human pulmonary microvascular endothelial cells: development of an alveolo-capillary barrier in vitro. *Labor Invest* 2004;**84**:736–52
18. Bertin J, Guo Y, Wang L, Srinivasula SM, Jacobson MD, Poyet JL, Merriam S, Du MQ, Dyer MJ, Robison KE, DiStefano PS, Alnemri ES. CARD9 is a novel caspase recruitment domain-containing protein that interacts with BCL10/CLAP and activates NF-kappa. *J Biol Chem* 2000;**275**:41082–6
19. Schmittgen KJLaTD. Analysis of relative gene expression data using realtime quantitative PCR and the 22DDCT method. *Methods* 2001;**25**:402–8
20. Ampawong S, Chaisri U, Viriyavejakul P, Prapansilp P, Grau GE, Turner GD, Pongponratn E. A potential role for interleukin-33 and gamma-epithelium sodium channel in the pathogenesis of human malaria associated lung injury. *Malar J* 2015;**14**:389
21. Ravichandran K, Tyagi A, Deep G, Agarwal C, Agarwal R. Interleukin-1beta-induced iNOS expression in human lung carcinoma A549 cells: involvement of STAT and MAPK pathways. *Indian J Exp Biol* 2011;**49**:840–7
22. Boost KA, Sadik CD, Bachmann M, Zwissler B, Pfeilschifter J, Mühl H. IFN-gamma impairs release of IL-8 by IL-1beta-stimulated A549 lung carcinoma cells. *BMC Cancer* 2008;**81**: 265
23. Song J, Zhao H, Dong H, Zhang D, Zou M, Tang H, Liu L, Liang Z, Lv Y, Zou F, Cai S. Mechanism of E-cadherin redistribution in bronchial airway epithelial cells in a TDI-induced asthma model. *Toxicol Lett* 2013;**220**:8–14
24. Schmiedl A, Ochs M, Muhlfeld C, Johnen G, Brasch F. Distribution of surfactant proteins in type II pneumocytes of newborn, 14-day old, and adult rats: an immunoelectron microscopic and stereological study. *Histochem Cell Biol* 2005;**124**:465–76

25. Anstey NM, Jacups SP, Cain T, Pearson T, Ziesing PJ, Fisher DA. Pulmonary manifestations of uncomplicated falciparum and vivax malaria: cough, small airways obstruction, impaired gas transfer, and increased pulmonary phagocytic activity. *J Infect Dis* 2002;**185**:1326–34
26. Deroost K, Tyberghein A, Lays N, Noppen S, Schwarzer E, Vanstreels E, Komuta M, Prato M, Lin JW, Pamplona A, Janse CJ, Arese P, Roskams T, Daelemans D, Opdenakker G, Van den Steen PE. Hemozoin induces lung inflammation and correlates with malaria-associated acute respiratory distress syndrome. *Am J Respir Cell Mol Biol* 2013;**48**:589–600
27. Jaramillo M, Plante I, Ouellet N, Vandal K, Tessier PA, Olivier M. Hemozoin-inducible proinflammatory events in vivo: potential role in malaria infection. *J Immunol* 2004;**172**:3101–10
28. Olivier M, Van Den Ham K, Shio MT, Kassa FA, Fougeray S. Malarial pigment hemozoin and the innate inflammatory response. *Front Immunol* 2014;**5**:25
29. Perl M, Lomas-Neira J, Chung CS, Ayala A. Epithelial cell apoptosis and neutrophil recruitment in acute lung injury-a unifying hypothesis? What we have learned from small interfering RNAs. *Mol Med* 2008; **14**: 465–75
30. Perl M, Chung CS, Perl U, Thakkar R, Lomas-Neira J, Ayala A. Therapeutic accessibility of caspase-mediated cell death as a key pathomechanism in indirect acute lung injury. *Crit Care Med* 2010;**38**:1179–86
31. Galani V, Tatsaki E, Bai M, Kitsoulis P, Lekka M, Nakos G, Kanavaros P. The role of apoptosis in the pathophysiology of Acute Respiratory Distress Syndrome (ARDS): an up-to-date cell-specific review. *Pathol Res Pract* 2010;**206**:145–50
32. Hara H, Ishihara C, Takeuchi A, Xue L, Morris SW, Penninger JM, Yoshida H, Saito T. Cell type-specific regulation of ITAM-mediated NF-kappaB activation by the adaptors, CARMA1 and CARD9. *J Immunol* 2008;**181**:918–30
33. Dorhoi A, Desel C, Yeremeev V, Pradl L, Brinkmann V, Mollenkopf HJ, Hanke K, Gross O, Ruland J, Kaufmann SHE. The adaptor molecule CARD9 is essential for tuberculosis control. *J Exp Med* 2010;**207**:777–92
34. Punsawad C, Maneerat Y, Chaisri U, Nantavisai K, Viriyavejakul P. Nuclear factor kappa B modulates apoptosis in the brain endothelial cells and intravascular leukocytes of fatal cerebral malaria. *Malar J* 2013;**12**:260
35. Punsawad C, Viriyavejakul P. Nuclear factor kappa B in urine sediment: a useful indicator to detect acute kidney injury in Plasmodium falciparum malaria. *Malar J* 2014;**13**:84
36. Viriyavejakul P, Khachonsaksumet V, Punsawad C. Liver changes in severe Plasmodium falciparum malaria: histopathology, apoptosis and nuclear factor kappa B expression. *Malar J* 2014;**13**:106
37. Coronado LM, Nadovich CT, Spadafora C. Malarial hemozoin: from target to tool. *Biochim Biophys Acta* 2014;**1840**:2032–41
38. Schwarzer E, Turrini F, Ulliers D, Giribaldi G, Ginsburg H, Arese P. Impairment of macrophage functions after ingestion of Plasmodium falciparum-infected erythrocytes or isolated malarial pigment. *J Exp Med* 1992;**176**:1033–41
39. Noland GS, Briones N, Sullivan DJ. Jr. The shape and size of hemozoin crystals distinguishes diverse Plasmodium species. *Mol Biochem Parasitol* 2003;**130**:91–9
40. Z'Graggen BR, Tornic J, Müller-Edenborn B, Reyes L, Booy C, Beck-Schimmer B. Acute lung injury: apoptosis in effector and target cells of the upper and lower airway compartment. *Clin Exp Immunol* 2010;**161**:324–31
41. Martin TR, Hagimoto N, Nakamura M, Matute BG. Apoptosis and epithelial injury in the lungs. *Proc Am Thorac Soc* 2005;**2**:214–20
42. Rieger AM, Nelson KL, Konowalchuk JD, Barreda DR. Modified annexin V/propidium iodide apoptosis assay for accurate assessment of cell death. *J Vis Exp* 2011;**50**:pii:2597
43. Crowley LC, Marfell BJ, Scott AP, Waterhouse NJ. Quantitation of apoptosis and necrosis by annexin v binding, propidium iodide uptake, and flow cytometry. *Cold Spring Harb Protoc* 2016;**2016**:pdb.prot087288
44. West JB. Comparative physiology of the pulmonary blood-gas barrier: the unique avian solution. *Am J Physiol* 2009;**297**:R1625R34
45. Vermeer PD, Denker J, Estin M, Moninger TO, Keshavjee S, Karp P, Kline JN, Zabner J. MMP9 modulates tight junction integrity and cell viability in human airway epithelia. *Am J Physiol* 2009;**296**:L751L62
46. Douglas IS, Diaz del Valle F, Winn RA, Voelkel NF. Beta-catenin in the fibroproliferative response to acute lung injury. *Am J Respir Cell Mol Biol* 2006;**34**:274–85
47. Hoang AN, Sandlin RD, Omar A, Egan TJ, Wright DW. The neutral lipid composition present in the digestive vacuole of Plasmodium falciparum concentrates heme and mediates β-hematin formation with an unusually low activation energy. *Biochemistry* 2010;**49**:10107–16
48. Scaccabarozzi D, Deroost K, Lays N, Omodeo Sale F, Van den Steen PE, Taramelli D. Altered lipid composition of surfactant and lung tissue in murine experimental malaria-associated acute respiratory distress syndrome. *PLoS One* 2015;**10**:e0143195
49. Li Q, Han Y, Du J, Jin H, Zhang J, Niu M, Qin J. Alterations of apoptosis and autophagy in developing brain of rats with epilepsy: changes in LC3, P62, Beclin-1 and Bcl-2 levels. *Neurosci Res* 2017. Epub ahead of print 12 August. DOI: 10.1016/j.neures.2017.08.004.
50. Scherz-Shouval R, Weidberg H, Gonen C, Wilder S, Elazar Z, Oren M. p53-dependent regulation of autophagy protein LC3 supports cancer cell survival under prolonged starvation. *Proc Natl Acad Sci USA* 2010;**107**:18511–6
51. Lin L, Zhang L, Yu L, Han L, Ji W, Shen H, Hu Z. Time-dependent changes of autophagy and apoptosis in lipopolysaccharide-induced rat acute lung injury. *Iran J Basic Med Sci* 2016;**19**:632–7

(Received December 21, 2017, Accepted January 15, 2018)